Transmission eigenvalues for the electromagnetic scattering problem in pseudo-chiral media and a practical reconstruction method

Tiexiang Li

School of Mathematics, Southeast University, Nanjing 211189, People's Republic of China.

E-mail: `txli@seu.edu.cn`

Tsung-Ming Huang

Department of Mathematics, National Taiwan Normal University, Taipei 116, Taiwan.

E-mail: `min@ntnu.edu.tw`

Wen-Wei Lin

Department of Applied Mathematics, National Chiao Tung University, Hsinchu 300, Taiwan.

E-mail: `wwlin@math.nctu.edu.tw`

Jenn-Nan Wang

Institute of Applied Mathematical Sciences, NCTS, National Taiwan University, Taipei, 106, Taiwan.

E-mail: `jnwang@math.ntu.edu.tw`

Abstract. In this paper, we consider the two-dimensional Maxwell's equations with the TM mode in pseudo-chiral media. The system can be reduced to the acoustic equation with a negative index of refraction. We first study the transmission eigenvalue problem (TEP) for this equation. By the continuous finite element method, we discretize the reduced equation and transform the study of TEP to a quadratic eigenvalue problem by deflating all nonphysical zeros. We then estimate half of the eigenvalues are negative with order of $O(1)$ and the other half of eigenvalues are positive with order of $O(10^2)$. In the second part of the paper, we present a practical numerical method to reconstruct the support of the inhomogeneity by the near-field measurements, i.e., Cauchy data. Based on the linear sampling method, we propose the truncated singular value decomposition to solve the ill-posed near-field integral equation, at one wave number which is not a transmission eigenvalue. By carefully chosen an indicator function, this method produce different jumps for the sampling points inside and outside the support. Numerical results show that our method is able to reconstruct the support reliably.

Keywords: Two-dimensional transmission eigenvalue problem, pseudo-chiral model, transverse magnetic mode, linear sampling method, singular value decomposition

1. Introduction

The transmission eigenvalue problem (TEP) has attracted a lot of attention recently in the study of direct/inverse scattering problems in inhomogeneous media [3, 4, 5, 6, 9, 11, 12, 20, 25]. The existence of transmission eigenvalues is intimately connected to the "bijectivity" of the far-field operator, which is crucial in some reconstruction methods such as the linear sampling method (LSM) [1, 8] and the factorization method [21]. Conversely, the transmission eigenvalues (also eigenvalues) carry the information of the scatterer and can be estimated by the far-field data [2] or the near-field data (Cauchy data) [27]. This observation leads to the development of some reconstruction methods using the transmission eigenvalues or eigenvalues, see for example, [10, 29]. In [29], an eigenvalue method using multiple frequency near-field data (EM^{2}F) was proposed to detect Dirichlet or transmission eigenvalues and to reconstruct the support of the scatterer.

In this paper, we would like to propose a reliable numerical method to investigate the distribution of transmission eigenvalues for the 2d acoustic equation with an inhomogeneous index of refraction. The model is derived from the Maxwell's equations with the TM mode in pseudo-chiral media. It turns out the index of refraction of the reduced acoustic equation decreases to negative infinity when we increase the charity parameter. Precisely, we consider the TEP

$$\Delta u + \lambda\varepsilon(\mathbf{x})u = 0, \quad \text{in } D, \tag{1a}$$
$$\Delta v + \lambda v = 0, \quad \text{in } D, \tag{1b}$$
$$u - v = 0, \quad \text{on } \partial D, \tag{1c}$$
$$\frac{\partial u}{\partial \boldsymbol{\nu}} - \frac{\partial v}{\partial \boldsymbol{\nu}} = 0, \quad \text{on } \partial D \tag{1d}$$

for the scattering of acoustic wave on a bounded and simply connected inhomogeneous domain $D \subseteq \mathbb{R}^2$, where $\boldsymbol{\nu}$ is the outer normal to the smooth boundary ∂D, $u, v \in L^2(D)$ with $u - v \in H_0^2(D) = \{w \in H^2 | w = 0, \frac{\partial w}{\partial \nu} = 0\}$, and $\varepsilon(\mathbf{x})$ is the index of refraction. Any $\lambda \in \mathbb{C}$ such that (1) has nontrivial solutions u and v is called a transmission eigenvalue and u, v are called the corresponding transmission eigenfunctions for D .

Equation (1a) can be considered as a reduced Maxwell's equations with transverse magnetic (TM) mode. For the standard Maxwell's equations, $\varepsilon(\mathbf{x})$ is the electric permittivity corresponding to the product of the dielectric constant and the free-space dielectric constant. In practice, ε can not be taken as large as we wish. In [23] where the Maxwell's equations for Tellegen media is studied, $\varepsilon(\mathbf{x})$ is the sum of the electric permittivity and the square of Tellegen parameter. By choosing large Tellegen parameter, we can enlarge the parameter $\varepsilon(\mathbf{x})$ as we want. On the contrary, here $\varepsilon(\mathbf{x})$ is the sum of the electric permittivity minus the square of pseudo-chiral media parameters. Therefore, by selecting the pseudo-chiral parameters sufficiently large, $\varepsilon(\mathbf{x})$ becomes negative (see Section 2 below).

In recent years, several papers have been devoted to developing efficient algorithms for computing transmission eigenvalues of 2d/3d TEP [3, 11, 14, 16, 17, 20, 21, 22, 23, 24, 26, 27]. Three finite element methods (FEMs) and a coupled boundary element method were developed to solve the 2d/3d TEP in [11, 14, 17] (see the book [30] for more details). Two iterative methods and the corresponding convergence analysis were given in [28]. In [17], a mixed finite element method for 2d TEP was proposed, which leads to a non-Hermitian quadratic eigenvalue problem (QEP) that was solved by an adaptive Arnoldi method. Furthermore, a multilevel correction method was used to reduce the solution of TEP into some linear boundary value problems which could be solved by the multigrid method [18]. For results related to our current work, in [23, 24], the TEP for general inhomogeneous media are discretized into QEP with symmetric coefficient matrices. For such QEP, a secant-type iteration for computing several smallest positive transmission eigenvalues accurately was proposed in [24], and a quadratic Jacobi-Davidson method with nonequivalent deflation technique for computing a large number positive transmission eigenvalues was developed in [23]. Remind that the index of refraction $\varepsilon(\mathbf{x})$ increases to infinity as we increase the Tellegen parameter. Numerical simulations demonstrate that the positive transmission eigenvalues are densely distributed in an interval near the origin. Similar to the method in [23], the TEP (1) is discretized into a QEP and a quadratic Jacobi-Davidson method with nonequivalence deflation is applied to compute a large number of positive eigenvalues. It turns out in the case here there exists an eigenvalue-free interval near the origin. The existence of the eigenvalue-free interval motivates us to study the reconstruction of the support of $\varepsilon(\mathbf{x})$ from the near-field data in the spirit of LSM.

Corresponding to the TEP(1), the scattering problem is described by

$$\Delta u + k^2\varepsilon(\mathbf{x})u = 0, \quad \text{in } \mathbb{R}^2 \setminus \{\mathbf{x}_0\}, \tag{2a}$$

$$u = u^i + u^s, \tag{2b}$$

$$\lim_{r\to\infty} \sqrt{r}\left(\frac{\partial u^s}{\partial r} - \mathrm{i}ku^s\right) = 0, \tag{2c}$$

where $D := \mathrm{supp}(\varepsilon(\mathbf{x}) - 1)$ and u^i is the incident field due to a point source at $\mathbf{x}_0$, i.e.,

$$u^i(\mathbf{x}, \mathbf{x}_0) := \Phi(\mathbf{x}, \mathbf{x}_0), \quad \mathbf{x}_0 \in C, \tag{3}$$

where $\Phi(\mathbf{x}, \mathbf{x}_0) = \frac{i}{4}H_0^{(0)}(k|\mathbf{x} - \mathbf{x}_0|)$, the fundamental solution of the Helmholtz equation in $\mathbb{R}^2$.

Our reconstruction method is based on the set up in [29]. We assume that the target D is inside some domain Ω which itself is inside a curve C (see Figure 1). Suppose that u^s is measured on $\Gamma = \partial\Omega$ for all point sources $\mathbf{x}$ on C. We define the near-field operator $\mathcal{N} : L^2(\Gamma) \to L^2(C)$ for $v \in L^2(\Gamma)$ by

$$(\mathcal{N}v)(\mathbf{x}) = \int_\Gamma u^s(\mathbf{y}, \mathbf{x})v(\mathbf{y})ds(\mathbf{y}), \quad \mathbf{x} \in C. \tag{4}$$

The LSM with near-field data relies on solving the ill-posed integral equations

$$(\mathcal{N}v)(\mathbf{x}) = \Phi(\mathbf{x}, \mathbf{z}) \quad \text{for all } \mathbf{x} \in C, \tag{5}$$

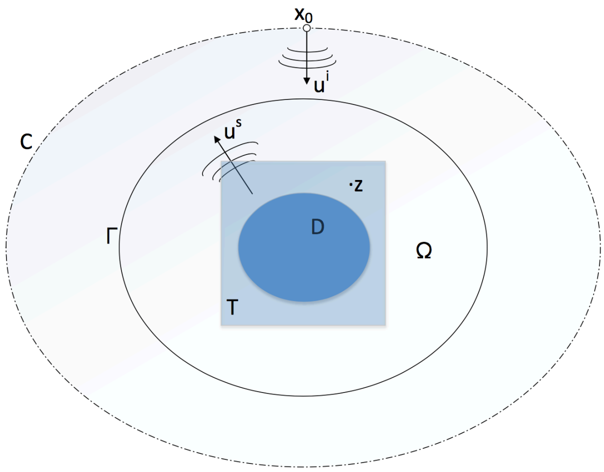

Figure 1. The target D is inside some domain Ω ($\Gamma := \partial\Omega$) which itself is surrounded by a curve C. The scattered field u^s is due to the scattering of the incident field u^i having a point source at $\mathbf{x}_0 \in C$.

where $\mathbf{z} \in T$ is a sampling point and T is a sampling domain inside Ω containing the target D (see Figure 1). In general, the above ill-posed equation do not have a solution. The following theorem serves as the backbone of the LSM.

Theorem 1.1. [8, 7, 29] *Assume that $\lambda = k^2$ is not a transmission eigenvalue of (1). Let $\mathcal{N}$ be the near-field operator defined by (4).*

- *If $\mathbf{z} \in D$, then there exists a convergent sequence v_n in $L^2(D)$, such that*

$$\lim_{n\to\infty} \mathcal{N} v_n = \Phi(\cdot, \mathbf{z}).$$

- *If $\mathbf{z} \in \Omega \setminus D$, then for every sequence v_n satisfying*

$$\lim_{n\to\infty} \mathcal{N} v_n = \Phi(\cdot, \mathbf{z}),$$

  we have

$$\lim_{n\to\infty} ||v_n||_{L^2(D)} = \infty.$$

Our reconstruction method is a direct application of Theorem 1.1. By this theorem, we can see that if k^2 is not a transmission eigenvalue then we can determine whether $\mathbf{z} \in D$ or $\mathbf{z} \in \Omega \setminus D$ from the behaviors of the solutions to (4). Since there exists an eigenvalue-free interval near the origin in TEP (1), we choose a k near the origin so that k^2 is not a transmission eigenvalue, we then discretize the integral equation (5). The strategy here is to choose m points $\mathbf{x}_1, \cdots, \mathbf{x}_m \in C$ forming a m-vector $\mathbf{b} = [\Phi(\mathbf{x}_1, \mathbf{z}), \cdots, \Phi(\mathbf{x}_m, \mathbf{z})]^\top \in \mathbb{C}^m$ and n unknowns $[v(\mathbf{y}_1), \cdots, v(\mathbf{y}_n)]^\top := \mathbf{v}$ satisfying the linear system

$$A\mathbf{v} = \mathbf{b}. \tag{6}$$

The idea is to take $m \geq n$, i.e., (6) is overdetermined. To determine whether $\mathbf{z} \in D$ or $\mathbf{z} \in \Omega \setminus D$, we look at the distance between the vector $\mathbf{b}$ and the space $\mathcal{A} = \text{span}(A)$, the subspace spanned by the columns of A, namely,

$$\text{dist}(\mathbf{b}, \mathcal{A}) \equiv \min_{\mathbf{v} \in \mathbb{C}^n} ||A\mathbf{v} - b||_2.$$

If $\text{dist}(\mathbf{b}, \mathcal{A}) > 0$, then, intuitively, any "solution" $\mathbf{v}$ satisfying (6) must contain some sufficiently large components. Mimicing the second case of Theorem 1.1, we thus assign $\mathbf{z} \in \Omega \setminus D$. On the other hand, if $\text{dist}(\mathbf{b}, \mathcal{A}) = 0$, i.e., $\mathbf{b} \in \mathcal{A}$, then the norm of $\mathbf{v}$ is clearly finite. We thus say that $\mathbf{z} \in D$ in view of the first case of Theorem 1.1. An easy application of truncated SVD will quickly determine the value of $\text{dist}(\mathbf{b}, \mathcal{A})$. Our criterion is very simple and easily to be implemented.

This paper is organized as follows. In Section 2, we demonstrate the derivation of 2d TEP (1) from the Maxwell's equations with TM mode in pseudo-chiral media. A corresponding discretized QEP and its spectral analysis are given in Section 3. In Section 4, a practical numerical method based on the LSM and truncated SVD for the reconstruction of the the target D is developed. Related numerical results are presented in Section 5. A concluding remark is given in Section 6. Finally, in Appendix A, we present a framework of solving the direct scattering problem using FEM. The purpose of solving the direct problem is to obtain synthetic data for numerical simulations.

2. Maxwell's equations with the TM mode in pseudo-chiral media

Physically, the governing equations for the propagation of electromagnetic wave in bi-isotropic materials with complex media is modeled by the 3d source-free frequency domain Maxwell's equations

$$\nabla \times E = \mathrm{i}k\left(\mu H + \zeta E\right), \tag{7a}$$

$$\nabla \times H = -\mathrm{i}k\left(\varepsilon_r E + \xi H\right), \tag{7b}$$

where E and H are the electronic field and magnetic field respectively, k is the frequency, ε_r and μ are electric permittivity and magnetic permeability respectively, ξ and ζ are 3-by-3 magnetoelectric parameter matrices in various forms for describing different types of complex media.

We consider E and H in (7) in the transversal magnetic (TM) mode as

$$E = [0, 0, E_3(\mathbf{x})]^\top, \;\; H = [H_1(\mathbf{x}), H_2(\mathbf{x}), 0]^\top \tag{8}$$

with $\mathbf{x} = (x_1, x_2)^\top \in \mathbb{R}^2$, ζ and ξ are pseudo-chiral media of the forms

$$\zeta = \begin{bmatrix} 0 & 0 & \zeta_1 \\ 0 & 0 & \zeta_2 \\ -\zeta_1 & -\zeta_2 & 0 \end{bmatrix}, \quad \xi = \begin{bmatrix} 0 & 0 & \xi_1 \\ 0 & 0 & \xi_2 \\ -\xi_1 & -\xi_2 & 0 \end{bmatrix} \tag{9}$$

with $\xi_1 = \zeta_1 = \mathrm{i}\gamma_1$, $\xi_2 = \zeta_2 = \mathrm{i}\gamma_2$, and γ_1, γ_2 being real numbers. We assume in this paper $\mu = 1$. Then the equation (7a) can be simplified to

$$\begin{bmatrix} \partial_{x_2} E_3 \\ -\partial_{x_1} E_3 \\ 0 \end{bmatrix} = \mathrm{i}k \left(\begin{bmatrix} H_1 \\ H_2 \\ 0 \end{bmatrix} + \begin{bmatrix} \zeta_1 E_3 \\ \zeta_2 E_3 \\ 0 \end{bmatrix} \right). \tag{10}$$

Substituting (10) into (7b) yields

$$\begin{aligned} (\mathrm{i}k)^{-1} & \begin{bmatrix} 0 \\ 0 \\ -\left(\frac{\partial^2}{\partial x_1^2} + \frac{\partial^2}{\partial x_2^2}\right) E_3 \end{bmatrix} - \begin{bmatrix} 0 \\ 0 \\ \frac{\partial}{\partial x_1}(\zeta_2 E_3) - \frac{\partial}{\partial x_2}(\zeta_1 E_3) \end{bmatrix} \\ = & -\mathrm{i}k \left(\varepsilon_r \begin{bmatrix} 0 \\ 0 \\ E_3 \end{bmatrix} - \begin{bmatrix} 0 \\ 0 \\ \xi_1 H_1 + \xi_2 H_2 \end{bmatrix} \right), \end{aligned}$$

which implies that

$$\begin{aligned} & -\Delta E_3 \\ = & k^2 \left[\varepsilon_r E_3 - \xi_1 \left((\mathrm{i}k)^{-1} \frac{\partial}{\partial x_2} E_3 - \zeta_1 E_3 \right) + \xi_2 \left((\mathrm{i}k)^{-1} \frac{\partial}{\partial x_1} E_3 + \zeta_2 E_3 \right) \right] \\ & + \mathrm{i}k \left[\frac{\partial}{\partial x_1}(\zeta_2 E_3) - \frac{\partial}{\partial x_2}(\zeta_1 E_3) \right] \\ = & k^2 (\varepsilon_r + \xi_1 \zeta_1 + \xi_2 \zeta_2) E_3 + \mathrm{i}k \left[\frac{\partial}{\partial x_1}(\zeta_2 E_3) - \frac{\partial}{\partial x_2}(\zeta_1 E_3) + \xi_1 \frac{\partial}{\partial x_2} E_3 - \xi_2 \frac{\partial}{\partial x_1} E_3 \right] \\ = & k^2 (\varepsilon_r - \gamma_1^2 - \gamma_2^2) E_3 \\ = & k^2 \varepsilon E_3 \end{aligned}$$

with $\varepsilon = \varepsilon_r - (\gamma_1^2 + \gamma_2^2)$.

Let $E_0 = [0, 0, E_{0,3}(\mathbf{x})]^\top$ and $H_0 = [H_{0,1}(\mathbf{x}), H_{0,2}(\mathbf{x}), 0]^\top$ be, respectively, the electronic and magnetic plane waves with TM mode in vacuum which are governed by the free Maxwell's equations

$$\nabla \times E_0 = \mathrm{i}k\mu_0 H_0, \tag{11a}$$

$$\nabla \times H_0 = -\mathrm{i}k\varepsilon_0 E_0 \tag{11b}$$

with $\varepsilon_0 = \mu_0 = 1$. We now suppose the Maxwell's equations (7) and (11) are defined on a cylindrical set $D \times \mathbb{R}$ satisfying the boundary conditions

$$E \times \widetilde{\boldsymbol{\nu}} = E_0 \times \widetilde{\boldsymbol{\nu}}, \tag{12a}$$

$$(H + \zeta E) \times \widetilde{\boldsymbol{\nu}} = H_0 \times \widetilde{\boldsymbol{\nu}}, \tag{12b}$$

where $\widetilde{\boldsymbol{\nu}} = [\nu_1, \nu_2, 0]^\top = [\boldsymbol{\nu}, 0]^\top$ is the outer unit normal to the smooth boundary $\partial D \times \mathbb{R}$. It is easily seen from (12a) that the Dirchlet boundary condition

$$E_3 = E_{0,3} \quad \text{on} \quad \partial D \tag{13a}$$

holds. Multiplying (12b) by ik and using (11a) we get the Neumann boundary condition

$$\nabla \times E \times \widetilde{\boldsymbol{\nu}} = \nabla \times E_0 \times \widetilde{\boldsymbol{\nu}},$$

i.e.,

$$\frac{\partial E_3}{\partial \boldsymbol{\nu}} = \frac{\partial E_{0,3}}{\partial \boldsymbol{\nu}} \quad \text{on} \;\; \partial D. \tag{13b}$$

In view of the boundary conditions (13a), (13b), choosing $u = E_3$ and $v = E_{0,3}$, we arrive at the TEP (1) with $\lambda = k^2$ and $\varepsilon(\mathbf{x}) = \varepsilon_r - (\gamma_1^2 + \gamma_2^2)$. The index of refraction will become negative as long as either $|\gamma_1|$ or $|\gamma_2|$ are sufficiently large.

3. Spectral analysis of discretized TEP

In this section, we first briefly introduce the discretized TEP and give its spectral analysis. Let $\{\phi_i\}_{i=1}^n$ and $\{\psi_i\}_{i=1}^m$ be standard nodal bases for spaces of continuous piecewise linear functions on $D \subset \mathbb{R}^2$, that have vanishing DoF on ∂D and D, respectively, where DoF denotes the degree of freedom. Applying the standard piecewise linear FEM (we refer to [11] for details) to (1) with

$$u = \sum_{i=1}^{n} u_i\phi_i + \sum_{i=1}^{m} w_i\psi_i, \tag{14a}$$

$$v = \sum_{i=1}^{n} v_i\phi_i + \sum_{i=1}^{m} w_i\psi_i. \tag{14b}$$

Hereafter, we denote 0 and I as a zero matrix/submatrix and the identity matrix, respectively, with appropriate dimensions if it is clear in the context. Now, setting $\mathbf{u} = [u_1, \cdots, u_n]^\top$, $\mathbf{v} = [v_1, \cdots, v_n]^\top$ and $\mathbf{w} = [w_1, \cdots, w_m]^\top$ appeared in (14), we can derive a generalized eigenvalue problem (GEP)

$$\mathcal{L}(\lambda)\mathbf{z} = (\mathcal{A} - \lambda\mathcal{B})\mathbf{z} = 0, \tag{15}$$

in which $\lambda = k^2$, where

$$\mathcal{A} = \begin{bmatrix} K & 0 & E \\ 0 & K & E \\ E^\top & -E^\top & 0 \end{bmatrix}, \; \mathcal{B} = \begin{bmatrix} -M_\varepsilon & 0 & -F_\varepsilon \\ 0 & M_1 & F_1 \\ -F_\varepsilon^\top & -F_1^\top & -G_\varepsilon - G_1 \end{bmatrix}, \; \mathbf{z} = \begin{bmatrix} \mathbf{u} \\ \mathbf{v} \\ \mathbf{w} \end{bmatrix} \tag{16}$$

with K, E, M_1, M_ε, F_1, F_ε, G_1 and G_ε being given in Table 1. Here, $A \succ 0$ means A is symmetric positive definite.

We now define

$$M = M_\varepsilon + M_1 \succ 0, \quad G = G_\varepsilon + G_1 \succ 0, \quad F = F_\varepsilon + F_1, \tag{17a}$$

$$\widehat{K} = K - EG^{-1}F^\top, \quad \widehat{M}_1 = M_1 - F_1G^{-1}F^\top, \quad \widehat{M} = M - FG^{-1}F^\top, \tag{17b}$$

and

$$\mathcal{S} = \begin{bmatrix} K & E \end{bmatrix}, \quad \mathcal{T}_1 = \begin{bmatrix} M_1 & F_1 \end{bmatrix}, \quad \mathcal{M} = \begin{bmatrix} M & F \\ F^\top & G \end{bmatrix}. \tag{17c}$$

stiffness matrix for interior meshes	$K = [(\nabla\phi_i, \nabla\phi_j)] \succ 0 \in \mathbb{R}^{n\times n}$
stiffness matrix for interior/boundary meshes	$E = [(\nabla\phi_i, \nabla\psi_j)] \in \mathbb{R}^{n\times m}$
mass matrices for interior meshes	$M_1 = [(\phi_i, \phi_j)] \succ 0 \in \mathbb{R}^{n\times n}$ $M_\varepsilon = [-(\varepsilon\phi_i, \phi_j)] \succ 0 \in \mathbb{R}^{n\times n}$
mass matrices for interior/boundary meshes	$F_1 = [(\phi_i, \psi_j)] \in \mathbb{R}^{n\times m}$ $F_\varepsilon = [-(\varepsilon\phi_i, \psi_j)] \in \mathbb{R}^{n\times m}$
mass matrices for boundary meshes	$G_1 = [(\psi_i, \psi_j)] \succ 0 \in \mathbb{R}^{m\times m}$ $G_\varepsilon = [-(\varepsilon\psi_i, \psi_j)] \succ 0 \in \mathbb{R}^{m\times m}$

Table 1. Stiffness and mass matrices with $\varepsilon(\mathbf{x}) < 0$ for $\mathbf{x} \in \bar{D}$.

Lemma 3.1. *Let M and $\widehat{M}$ be defined in (17a), (17b). Then $\mathcal{M}, \widehat{M} \succ 0$.*

Proof. Because

$$\begin{bmatrix} M_1 & F_1 \\ F_1^\top & G_1 \end{bmatrix} \succ 0, \quad \begin{bmatrix} M_\varepsilon & F_\varepsilon \\ F_\varepsilon^\top & G_\varepsilon \end{bmatrix} \succ 0,$$

we see that

$$\mathcal{M} = \begin{bmatrix} M & F \\ F^\top & G \end{bmatrix} = \begin{bmatrix} M_1 & F_1 \\ F_1^\top & G_1 \end{bmatrix} + \begin{bmatrix} M_\varepsilon & F_\varepsilon \\ F_\varepsilon^\top & G_\varepsilon \end{bmatrix} \succ 0.$$

On the other hand, observe that

$$0 \prec \begin{bmatrix} I & -FG^{-1} \\ 0 & I \end{bmatrix} \begin{bmatrix} M & F \\ F^\top & G \end{bmatrix} \begin{bmatrix} I & 0 \\ -G^{-1}F^\top & I \end{bmatrix} = \begin{bmatrix} \widehat{M} & 0 \\ 0 & G \end{bmatrix},$$

which implies $\widehat{M} \succ 0$. □

Theorem 3.2. *For $\lambda \neq 0$, the* GEP (15) *can be reduced to the following* QEP

$$\mathcal{Q}(\lambda)\mathbf{p} = (\lambda^2 A_2 - \lambda A_1 - A_0)\mathbf{p} = 0, \tag{18}$$

where $\mathbf{p} = \mathbf{u} - \mathbf{v}$, A_2, A_1 and A_0 are all $n \times n$ symmetric matrices given by

$$\begin{aligned} A_2 &= M_1 - \widehat{M}_1\widehat{M}^{-1}\widehat{M}_1^\top - F_1G^{-1}F_1^\top &\quad (19a)\\ &= M_1 - \mathcal{T}_1\mathcal{M}^{-1}\mathcal{T}_1^\top, \\ A_1 &= K - \widehat{K}\widehat{M}^{-1}\widehat{M}_1^\top - \widehat{M}_1\widehat{M}^{-1}\widehat{K}^\top - EG^{-1}F_1^\top - F_1G^{-1}E^\top &\quad (19b)\\ &= K - \mathcal{S}\mathcal{M}^{-1}\mathcal{T}_1^\top - \mathcal{T}_1\mathcal{M}^{-1}\mathcal{S}^\top, \\ A_0 &= \widehat{K}\widehat{M}^{-1}\widehat{K}^\top + EG^{-1}E^\top &\quad (19c)\\ &= \mathcal{S}\mathcal{M}^{-1}\mathcal{S}^\top. \end{aligned}$$

Proof. By (16), subtracting the 1st equation by the 2nd equation in (15), and rewriting the 3rd equation in (15) we have

$$\begin{bmatrix} K \\ E^\top \end{bmatrix} \mathbf{p} - \lambda \begin{bmatrix} M_1 \\ F_1^\top \end{bmatrix} \mathbf{p} = -\lambda \begin{bmatrix} M_\varepsilon + M_1 & F_\varepsilon + F_1 \\ F_\varepsilon^\top + F_1^\top & G_\varepsilon + G_1 \end{bmatrix} \begin{bmatrix} \mathbf{u} \\ \mathbf{v} \end{bmatrix}. \tag{20}$$

On the other hand, from the 1st equation of (15) and the 1st equation of (20), we have

$$\begin{bmatrix} K & E \end{bmatrix} \begin{bmatrix} \mathbf{u} \\ \mathbf{w} \end{bmatrix} - \lambda \begin{bmatrix} M_1 & F_1 \end{bmatrix} \begin{bmatrix} \mathbf{u} \\ \mathbf{w} \end{bmatrix} + \lambda M_1 \mathbf{p} = K\mathbf{p}. \tag{21}$$

From (17a) and (17c), equations (20) and (21) can be rewritten as

$$(\mathcal{S} - \lambda \mathcal{T}_1)^\top \mathbf{p} = -\lambda \mathcal{M} \begin{bmatrix} \mathbf{u} \\ \mathbf{w} \end{bmatrix}, \tag{22a}$$

$$(\mathcal{S} - \lambda \mathcal{T}_1) \begin{bmatrix} \mathbf{u} \\ \mathbf{w} \end{bmatrix} + \lambda M_1 \mathbf{p} = K\mathbf{p}. \tag{22b}$$

Expressing $\begin{bmatrix} \mathbf{u} \\ \mathbf{w} \end{bmatrix}$ in terms of $\mathbf{p}$ in (22a) and plugging it into (22b), we end up with a QEP

$$\left[\lambda^2 M_1 - (\mathcal{S} - \lambda \mathcal{T}_1)\mathcal{M}^{-1}(\mathcal{S} - \lambda \mathcal{T}_1)^\top\right] \mathbf{p} = \lambda K \mathbf{p}. \tag{23}$$

Rewriting (23) as

$$\left[\lambda^2 (M_1 - \mathcal{T}_1 \mathcal{M}^{-1} \mathcal{T}_1^\top) + \lambda(-K + \mathcal{S}\mathcal{M}^{-1}\mathcal{T}_1^\top + \mathcal{T}_1\mathcal{M}^{-1}\mathcal{S}^\top) - \mathcal{S}\mathcal{M}^{-1}\mathcal{S}^\top\right] \mathbf{p} = 0$$

and using the fact that

$$\mathcal{M}^{-1} = \begin{bmatrix} M & F \\ F^\top & G \end{bmatrix}^{-1} = \begin{bmatrix} \widehat{M}^{-1} & 0 \\ -G^{-1}F^\top \widehat{M}^{-1} & G^{-1} \end{bmatrix} \begin{bmatrix} I & -FG^{-1} \\ 0 & I \end{bmatrix}.$$

We can show by careful calculation that the coefficient matrices in (23) satisfy those in (19). □

Corollary 3.3. [15] *Let $\mathcal{L}(\lambda)$ and $\mathcal{Q}(\lambda)$ be defined in (15) and (18), respectively. Then*

$$\sigma(\mathcal{L}(\lambda)) = \sigma(\mathcal{Q}(\lambda)) \cup \{\underbrace{0, \cdots, 0}_{m}\},$$

where $\sigma(\cdot)$ denotes the spectra of the associated matrix pencil.

Theorem 3.4. *Let $\mathcal{Q}(\lambda)$ in (18) with matrices A_2, A_1 and A_0 defined in (19). Then A_2 and A_0 are positive definite. Furthermore there are n negative and n positive eigenvalues for $\mathcal{Q}(\lambda)$.*

Proof. From Lemma 3.1 and $\mathcal{S}^\top$ being of full column rank, we get that the matrix A_0 in (19c) is positive definite. On the other hand, from

$$\begin{bmatrix} M_1 & F_1 \\ F_1^\top & G_1 \end{bmatrix} \succ 0, \quad \begin{bmatrix} M_\varepsilon & F_\varepsilon \\ F_\varepsilon^\top & G_\varepsilon \end{bmatrix} \succ 0$$

it follows

$$\mathcal{C} \equiv \begin{bmatrix} M_1 & 0 & F_1 \\ 0 & 0 & 0 \\ F_1^\top & 0 & G_1 \end{bmatrix} + \begin{bmatrix} 0 & 0 & 0 \\ 0 & M_\varepsilon & F_\varepsilon \\ 0 & F_\varepsilon^\top & G_\varepsilon \end{bmatrix} = \begin{bmatrix} M_1 & 0 & F_1 \\ 0 & M_\varepsilon & F_\varepsilon \\ F_1^\top & F_\varepsilon^\top & G \end{bmatrix} \succ 0.$$

Let

$$L_1 = \begin{bmatrix} I_n & 0 & 0 \\ I_n & I_n & 0 \\ 0 & 0 & I_m \end{bmatrix}, \quad L_2 = \begin{bmatrix} I_n & 0 & 0 \\ 0 & I_n & -FG^{-1} \\ 0 & 0 & I_m \end{bmatrix},$$

$$L_3 = \begin{bmatrix} I_n & -\widehat{M}_1\widehat{M}^{-1} & 0 \\ 0 & I_n & 0 \\ 0 & 0 & I_m \end{bmatrix}, \quad L_4 = \begin{bmatrix} I_n & 0 & -F_1G^{-1} \\ 0 & I_n & 0 \\ 0 & 0 & I_m \end{bmatrix}.$$

Then

$$\begin{aligned}
0 &\prec L_4L_3L_2L_1\mathcal{C}L_1^\top L_2^\top L_3^\top L_4^\top \\
&= L_4L_3L_2 \begin{bmatrix} M_1 & 0 & F_1 \\ M_1 & M_\varepsilon & F \\ F_1^\top & F_\varepsilon^\top & G \end{bmatrix} \begin{bmatrix} I_n & I_n & 0 \\ 0 & I_n & 0 \\ 0 & 0 & I_m \end{bmatrix} L_2^\top L_3^\top L_4^\top \\
&= L_4L_3 \begin{bmatrix} M_1 & M_1 & F_1 \\ \widehat{M}_1^\top & \widehat{M} & 0 \\ F_1^\top & F^\top & 0 \end{bmatrix} \begin{bmatrix} I_n & 0 & 0 \\ 0 & I_n & 0 \\ 0 & -G^{-1}F^\top & I_m \end{bmatrix} L_3^\top L_4^\top \\
&= L_4 \begin{bmatrix} M_1 - \widehat{M}_1\widehat{M}^{-1}\widehat{M}_1^\top & 0 & F_1 \\ \widehat{M}_1^\top & \widehat{M} & 0 \\ F_1^\top & 0 & G \end{bmatrix} \begin{bmatrix} I_n & 0 & 0 \\ -\widehat{M}^{-1}\widehat{M}_1^\top & I_n & 0 \\ 0 & 0 & I_m \end{bmatrix} L_4^\top \\
&= \begin{bmatrix} A_2 & 0 & 0 \\ 0 & \widehat{M} & 0 \\ 0 & 0 & G \end{bmatrix},
\end{aligned}$$

which implies that $A_2 \succ 0$.

Let $(\lambda, \mathbf{p})$ be an eigenpair of (18), then

$$\lambda^2(\mathbf{p}^H A_2 \mathbf{p}) - \lambda(\mathbf{p}^H A_1 \mathbf{p}) - (\mathbf{p}^H A_0 \mathbf{p}) = 0. \tag{24}$$

Here and hereafter, the superscript "H" in (24) denotes the conjugate transpose. Because A_1 is symmetric and $A_2, A_0 \succ 0$, we have

$$a_2 \equiv \mathbf{p}^H A_2 \mathbf{p} > 0, \quad a_1 \equiv \mathbf{p}^H A_1 \mathbf{p} \in \mathbb{R}, \quad a_0 \equiv \mathbf{p}^H A_0 \mathbf{p} > 0, \tag{25}$$

which implies that the roots of the quadratic equation (24) are

$$\lambda_+ = \frac{a_1 + \sqrt{a_1^2 + 4a_2 a_0}}{2a_2} > 0, \quad \lambda_- = \frac{a_1 - \sqrt{a_1^2 + 4a_2 a_0}}{2a_2} < 0. \tag{26}$$

Hence, there are n negative and n positive eigenvalues for (18) and the associated eigenvectors are real vectors. $\square$

Theorem 3.5. *Let*

$$W_0 = \begin{bmatrix} M & F \\ F^\top & G \end{bmatrix}^{-1/2} \begin{bmatrix} K \\ E^\top \end{bmatrix}, \quad W_1 = \begin{bmatrix} M & F \\ F^\top & G \end{bmatrix}^{-1/2} \begin{bmatrix} M_1 \\ F_1^\top \end{bmatrix}, \tag{27}$$

and

$$d_0 = \|W_0\|_2, \quad d_1 = \|W_1\|_2.$$

Suppose that

$$\underline{a}_1 = \lambda_{\min}(K) - d_0 d_1 > 0, \tag{28a}$$

$$\underline{a}_0 = \lambda_{\min}(A_0), \quad \bar{a}_0 = \lambda_{\max}(A_0) = d_0^2, \tag{28b}$$

$$\underline{a}_2 = \lambda_{\min}\left(A_2\right), \quad \bar{a}_2 = \lambda_{\max}(A_2). \tag{28c}$$

Then the n negative and n positive eigenvalues of (18) are, respectively, in the intervals $(-\beta_*, 0)$ and (β^*, ∞), where

$$\beta_* = \frac{2\bar{a}_0}{\sqrt{\underline{a}_1^2 + 4\underline{a}_2\underline{a}_0} + \underline{a}_1}, \quad \beta^* = \frac{\underline{a}_1 + \sqrt{\underline{a}_1^2 + 4\underline{a}_2\underline{a}_0}}{2\bar{a}_2}. \tag{29}$$

Proof. By the definitions of W_0 and W_1, A_1 in (19b) can be represented as

$$A_1 = K - W_0^\top W_1 - W_1^\top W_0. \tag{30}$$

Given an orthogonal vector $\mathbf{p}$, from (27) and (28a), equation (30) implies that

$$\mathbf{p}^H A_1 \mathbf{p} = \mathbf{p}^H K \mathbf{p} - \mathbf{p}^H W_0^\top W_1 \mathbf{p} - \mathbf{p}^H W_1^\top W_0 \mathbf{p} \geq \lambda_{\min}(K) - d_0 d_1 = \underline{a}_1 > 0. \tag{31}$$

From (25)-(27) and (31), it follows that

$$-\lambda_- = \frac{2a_0}{\sqrt{a_1^2 + 4a_2 a_0} + a_1} \leq \frac{2\bar{a}_0}{\sqrt{\underline{a}_1^2 + 4\underline{a}_2\underline{a}_0} + \underline{a}_1} = \beta_*,$$

and

$$\lambda_+ = \frac{a_1 + \sqrt{a_1^2 + 4a_2 a_0}}{2a_2} \geq \frac{\underline{a}_1 + \sqrt{\underline{a}_1^2 + 4\underline{a}_2\underline{a}_0}}{2\bar{a}_2} = \beta^*.$$

$\square$

4. Numerical method for reconstructing the unknown domain

In this section, we will propose a practical numerical method for the reconstruction of the support of the target D based on the LSM and the truncated SVD technique. As described in the Introduction, let $\mathbf{z}$ be a sampling point in the sampling domain T (see Figure 1) and k^2 is not a transmission eigenvalue for TEP (1). According to Theorem 1.1, from (4) and (5), we can determine whether $\mathbf{z}$ is inside D or not by solving $v \in L^2(\Gamma)$ which satisfies the near field integral equation

$$\int_\Gamma u^s(\mathbf{x},\mathbf{y})v(\mathbf{y})ds(\mathbf{y}) = \Phi(\mathbf{x},\mathbf{z}) \quad \text{for all } \mathbf{x} \in C, \tag{32}$$

where $\Phi(\mathbf{x},\mathbf{z})$ is given in (3).

To solve (32), we first discretize (32) as follows. For each point source $\mathbf{x}_i \in C$, $i = 1, \cdots, m$, suppose we have measured the scattered fields on the discrete points $\mathbf{y}_1, \cdots, \mathbf{y}_n$ on Γ. With these scattered fields, the discretized equation of (32) can be formulated as the overdetermined linear system

$$A\mathbf{v} = \mathbf{b}, \tag{33}$$

where $\mathbf{b} = [\Phi(\mathbf{x}_1,\mathbf{z}), \cdots, \Phi(\mathbf{x}_m,\mathbf{z})]^\top \in \mathbb{C}^m$, $A \in \mathbb{C}^{m\times n}$ depends on $\mathbf{x}_i$ and $\mathbf{y}_j$ for $i = 1, \cdots, m$ and $j = 1, \cdots, n$, and the measured scattered fileds. $\mathbf{v} \in \mathbb{C}^n$ is the approximation to the unknown values $[v(\mathbf{y}_1), \cdots, v(\mathbf{y}_n)]^\top$. In general, the linear system (33) is very sensitive due to the ill-posedness of (32). For the case of $m < n$, the problem (33) can be solved by the Tikhonov regularization method which gives

$$\min_{\mathbf{v}\in\mathbb{C}^n} \{||A\mathbf{v} - \mathbf{b}||^2 + \delta||\mathbf{v}||^2\} \tag{34}$$

with $\delta > 0$ be a regularization parameter. The proper choice of regularization parameters plays an important role in (34) in order to achieve accurate and stable numerical results. Actually, over the last four decades, many different methods for selecting regularization parameters have been proposed [13, 19, 31]. Even so, the selection of the optimal regularization parameter remains a difficult question in solving the discretized ill-posed linear system (33).

In this paper, we will propose a novel numerical method to reconstruct the domain D by solving the linear system (33) for the case of $m \geq n$. Let $\mathcal{A} = \text{span}(A)$ be the subspace spanned by the columns of A. Recall from Section 1 that

$$\text{dist}(\mathbf{b}, \mathcal{A}) = \min_{\mathbf{v}\in\mathbb{C}^n} ||A\mathbf{v} - b||_2.$$

From the perspective of matrix analysis, we reinterpret Theorem 1.1 in the following way. Assume that k^2 is not an eigenvalue of (18), for instance, we choose $0 < k^2 < \beta^*$. If $\text{dist}(\mathbf{b}, \mathcal{A}) > 0$, then $\mathbf{v}$ satisfying (33) is in the sense that some components of $\mathbf{v}$ are infinity. In other words, we have $\|\mathbf{v}\| = \infty$. We then assign $\mathbf{z} \in \Omega \setminus D$. On the other hand, if $\text{dist}(\mathbf{b}, \mathcal{A}) = 0$, then we can find a regular vector $\mathbf{v}$ with $\|\mathbf{v}\| < \infty$ satisfying

(33). In this case, we say that $\mathbf{z} \in D$. Our reconstruction method is based on this interpretation.

We will use a truncated SVD to determine the size of $\mathbf{v}$. Let

$$A = U \begin{bmatrix} \Sigma \\ 0 \end{bmatrix} V^H$$

be the SVD of A, where $U \in \mathbb{C}^{m\times m}$ and $V \in \mathbb{C}^{n\times n}$ are unitary, $\Sigma = \mathrm{diag}(\sigma_1, \cdots, \sigma_n)$ is diagonal matrix of singular values with $\sigma_1 \geq \cdots \geq \sigma_n \geq 0$. Usually, the discretized linear system (33) is sensitive that is inherited from the ill-posedness of (32), and the coefficient matrix A in (33) is not of full column rank. Suppose $\mathrm{rank}(A) = r < n$, which means that $\sigma_r > \sigma_{r+1} = \cdots = \sigma_n = 0$. Denote $\Sigma_r = \mathrm{diag}(\sigma_1, \cdots, \sigma_r)$ and partition U and V with respect to Σ_r as $U = [U_1, U_2]$ and $V = [V_1, V_2]$ with $U_1 \in \mathbb{C}^{m\times r}$ and $V_1 \in \mathbb{C}^{n\times r}$, respectively. Obviously, the following statements hold true.

$$A = U_1 \Sigma_r V_1^H, \ \mathcal{A} = \mathrm{span}(U_1) \equiv \text{the subspace spanned by columns of } U_1, \tag{35}$$

and

$$\mathrm{dist}(\mathbf{b}, \mathcal{A})^2 = \min_{\mathbf{v}\in\mathbb{C}^n} ||A\mathbf{v} - \mathbf{b}||_2^2 = \min_{\mathbf{v}\in\mathbb{C}^r} ||\Sigma_r \mathbf{v} - U_1^H \mathbf{b}||_2^2 + ||U_2^H \mathbf{b}||_2^2 = ||U_2^H \mathbf{b}||_2^2,$$

where $U_1 \Sigma_r V_1^H$ is called the truncated SVD of A. Let $\mathbf{v}$ be a vector satisfying (33). Then we have

$$A\mathbf{v} = \mathbf{b} \Leftrightarrow \begin{bmatrix} \Sigma_r & 0 \\ 0 & 0 \end{bmatrix} \begin{bmatrix} V_1^H \mathbf{v} \\ V_2^H \mathbf{v} \end{bmatrix} = \begin{bmatrix} U_1^H \mathbf{b} \\ U_2^H \mathbf{b} \end{bmatrix} \equiv \begin{bmatrix} \Sigma_r & 0 \\ 0 & 0 \end{bmatrix} \begin{bmatrix} \hat{\mathbf{v}}_1 \\ \hat{\mathbf{v}}_2 \end{bmatrix} = \begin{bmatrix} \hat{\mathbf{b}}_1 \\ \hat{\mathbf{b}}_2 \end{bmatrix}. \tag{36}$$

We interpret that $v = \infty$ is the solution of the equation $0\,v = c$ if $c \neq 0$. Thus, from (36) follows that

$$\Sigma_r \hat{\mathbf{v}}_1 = \hat{\mathbf{b}}_1 \Rightarrow \hat{\mathbf{v}}_1 = \Sigma_r^{-1} \hat{\mathbf{b}}_1 \Rightarrow ||\hat{\mathbf{v}}_1|| < \infty,$$

and

$$0\hat{\mathbf{v}}_1 + 0\hat{\mathbf{v}}_2 = \hat{\mathbf{b}}_2 \Rightarrow \ \text{if } ||\hat{\mathbf{b}}_2|| \neq 0, \ \text{then } ||\hat{\mathbf{v}}|| = \infty.$$

This implies that

$$\text{if } \mathbf{b} \in \mathrm{span}\{U_1\} \Leftrightarrow \mathrm{rank}(A) = \mathrm{rank}([A, \mathbf{b}]), \ \text{then } ||\mathbf{v}|| < \infty; \tag{37a}$$

$$\text{if } \mathbf{b} \notin \mathrm{span}\{U_1\} \Leftrightarrow \mathrm{rank}(A) \neq \mathrm{rank}([A, \mathbf{b}]), \ \text{then } ||\mathbf{v}|| = \infty. \tag{37b}$$

On the other hand, let $\widehat{A} = [A, \mathbf{b}]$, then

$$\widehat{A}^H \widehat{A} = \begin{bmatrix} V_1 \Sigma_r & 0 \\ \hat{\mathbf{b}}_1^H & \hat{\mathbf{b}}_2^H \end{bmatrix} \begin{bmatrix} \Sigma_r V_1^H & \hat{\mathbf{b}}_1 \\ 0 & \hat{\mathbf{b}}_2 \end{bmatrix} = \begin{bmatrix} V_1 \Sigma_r^2 V_1^H & V_1 \Sigma_r \hat{\mathbf{b}}_1 \\ \hat{\mathbf{b}}_1^H \Sigma_r V_1^H & ||\mathbf{b}||_2^2 \end{bmatrix}. \tag{38}$$

It is easy to see that $\widehat{A}^H \widehat{A}$ in (38) is similar to

$$\begin{bmatrix} \Sigma_r^2 & \Sigma_r \hat{\mathbf{b}}_1 & 0 \\ \hat{\mathbf{b}}_1^H \Sigma_r & ||\mathbf{b}||_2^2 & 0 \\ 0 & 0 & 0 \end{bmatrix} \equiv \begin{bmatrix} \widehat{\Sigma}^2 & 0 \\ 0 & 0 \end{bmatrix} \tag{39}$$

by similarity transformations $V \oplus I$ and $0 \oplus \begin{bmatrix} 0 & I \\ I & 0 \end{bmatrix}$. Here "$\oplus$" denotes the direct sum of matrices. Let $\hat{\sigma}_1 \geq \cdots \geq \hat{\sigma}_{r+1} \geq 0$ be eigenvalues of $\widehat{\Sigma}$. It follows immediately that the singular values of $\widehat{A}$ are $\hat{\sigma}_1 \geq \cdots \geq \hat{\sigma}_{r+1} \geq \hat{\sigma}_{r+2} = \cdots = \hat{\sigma}_{n+1} = 0$.

In view of the special structure of matrix $\widehat{\Sigma}$ in (39), we apply the interlacing theorem for singular values of Σ and $\widehat{\Sigma}$ which leads to

$$\hat{\sigma}_1 \geq \sigma_1 \geq \hat{\sigma}_2 \geq \sigma_2 \geq \cdots \hat{\sigma}_r \geq \sigma_r \geq \hat{\sigma}_{r+1} \geq \sigma_{r+1} = 0. \tag{40}$$

For convenience, we set $0/0 = 1$. Let $\sigma_{n+1} = 0$, then we have

$$1 \leq \hat{\sigma}_j/\sigma_j < \infty \text{ for } j = 1, \cdots, r, \text{ and } \hat{\sigma}_j/\sigma_j = 1 \text{ for } j = r+2, \cdots, n+1. \tag{41}$$

Combing (40) and (41), the statements (37) can be represented as

$$\mathbf{b} \in \mathrm{span}\{U_1\} \Leftrightarrow \hat{\sigma}_{r+1} = 0, \text{ thus } \hat{\sigma}_{r+1}/\sigma_{r+1} = 0/0 = 1; \tag{42a}$$
$$\mathbf{b} \notin \mathrm{span}\{U_1\} \Leftrightarrow \hat{\sigma}_{r+1} \neq 0, \text{ thus } \hat{\sigma}_{r+1}/\sigma_{r+1} = \hat{\sigma}_{r+1}/0 = \infty. \tag{42b}$$

In conclusion, in our method, to decide whether $\mathbf{z} \in D$ or not relies heavily on effectively determining the ranks of A and $\widehat{A}$. However, since the integral equation (33) is ill-posed, the matrices A and $\widehat{A}$ are normally ill-conditioned and there is often no gap in the spectrums of singular values. From numerical point of view, it is difficult to compute the truncated SVD for A. Consequently, we usually set $r = n$.

We now propose a practical criterion to numerically realize (42). As above, let the singular values of A be $\sigma_1 \geq \cdots \geq \sigma_n \geq 0$ and those of $\widehat{A}$ be $\hat{\sigma}_1 \geq \cdots \geq \hat{\sigma}_{n+1} \geq 0$. We first compute

$$j(\mathbf{z}) \equiv \arg\max_{1 \leq j \leq n} \frac{\hat{\sigma}_j}{\sigma_j}$$

and define

$$I_{\mathbf{z}} = \hat{\sigma}_{j(\mathbf{z})}.$$

Here $I_{\mathbf{z}}$ is used as an indicator to determine whether $\mathbf{z}$ is in D or not. Precisely, we pick a small threshold parameter $0 < \mathrm{M}$. Then we choose the following dichotomy:

$$\begin{aligned} &\text{if } I_{\mathbf{z}} < \mathrm{M}, \text{ then we set } \mathbf{z} \in D, \\ &\text{if } I_{\mathbf{z}} \geq \mathrm{M}, \text{ then we set } \mathbf{z} \notin D. \end{aligned}$$

The algorithm of computing the indicator $I_{\mathbf{z}}$ is summarized in Algorithm 1 below.

5. Numerical experiments

In what follows, we will demonstrate the efficiency of our numerical method for four different domains shown in Figure 2: (a) a disk centered at $(0, 0)$ with radius 0.5; (b) an ellipse region centered at the origin with axes 0.6 and 0.4; (c) a peanut-like region

Algorithm 1 Practical numerical reconstruction method based on the singular values

Input: Discrete point sources $\mathbf{x}_i \in C$, detection points $\mathbf{y}_j \in \Gamma$ for $i = 1, \cdots, m$ and $j = 1, \cdots, n$, respectively, with $m > n$. The wave number $k \in \mathbb{R}$ and sampling points $\mathbf{z} \in T$.

Output: The indicator $I_{\mathbf{z}}$.

1: For each point sources $\mathbf{x}_i$, collect all the measured scattered field u^s_{ij} for $i = 1, \cdots, m, j = 1, \cdots, n$.

2: Using the measured scattered field u^s_{ij} to discretize the integral of (32), then construct the coefficient matrix $A \in \mathbb{C}^{m\times n}$ of (33).

3: Compute the SVD of $A = U_1 \Sigma_n V_1^H$ as in (35) with $\Sigma_n = \mathrm{diag}(\sigma_1, \cdots, \sigma_n)$.

4: For the sampling point $\mathbf{z}$, compute the vector on the right hand side of (33), $\mathbf{b} = [\Phi(\mathbf{x}_1, \mathbf{z}), \cdots, \Phi(\mathbf{x}_m, \mathbf{z})]^T$, where $\Phi(\cdot, \cdot)$ is given in (3).

5: Let $\widehat{\Sigma} \equiv \begin{bmatrix} \Sigma_n^2 & \Sigma_n \hat{\mathbf{b}}_1 \\ \hat{\mathbf{b}}_1^H \Sigma_n & \|\mathbf{b}\|_2^2 \end{bmatrix}$ with $\hat{\mathbf{b}}_1 = U_1^H \mathbf{b}$.

6: Calculate the singular values of $\widehat{\Sigma}$ as $\hat{\sigma}_1 \geq \cdots \geq \hat{\sigma}_{n+1}$.

7: Determine the index $j(\mathbf{z}) = \arg\max_{1\leq j\leq n} \hat{\sigma}_j/\sigma_j$.

8: Set $I_{\mathbf{z}} = \hat{\sigma}_{j(\mathbf{z})}$.

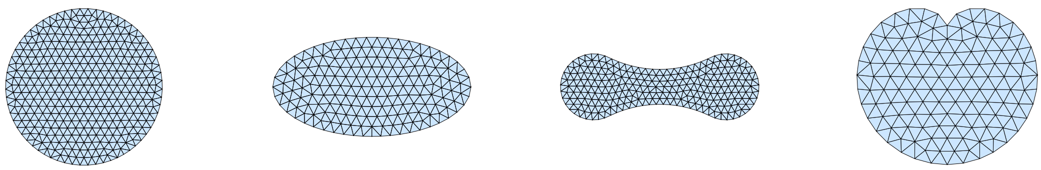

(a) Disk (b) Ellipse (c) Peanut (d) Heart

Figure 2. Four model domains that represent the region D.

enclosed by the equation $((x_1 - 0.7)^2 + x_2^2)((x_1 + 0.7)^2 + x_2^2) = 0.72^4$; (d) a heart-like region enclosed by the equation $x_1^2 + x_2^2 + 0.5x_2 = 0.5\sqrt{x_1^2 + x_2^2}$.

All computations for numerical test examples are carried out in MATLAB 2017a. For the hardware configuration, we use an HP server equipped with the RedHat Linux operating system, two Intel Quad-Core Xeon E5-2643 3.33 GHz CPUs and 96 GB of main memory.

5.1. Distribution of the transmission eigenvalues

We carry out the FEM method described in Section 3 to the TEP (1) on four different domains as in Figure 2 with the regular mesh size $h \approx 0.004$ for triangles of each domain D. We set $\varepsilon_r = 16$, $\gamma_1 = 10$, $\gamma_2 = 4$, and thus $\varepsilon(\mathbf{x}) = -100$. The associated dimensions n and m of matrices given in Table 1 are shown in Table 2. For each domain, we derive a corresponding QEP as given in (18).

Because of the two negative signs in (18), we should modify the quadratic Jacobi-

Table 2. Dimensions n, m ($K \in \mathbb{R}^{n\times n}$, $E \in \mathbb{R}^{n\times m}$) of matrices for the benchmark problems with the mesh size $h \approx 0.004$.

Domain	Disk	Ellipse	Peanut	Heart
(n, m)	(124631, 1150)	(71546, 976)	(149051, 1871)	(168548, 1492)

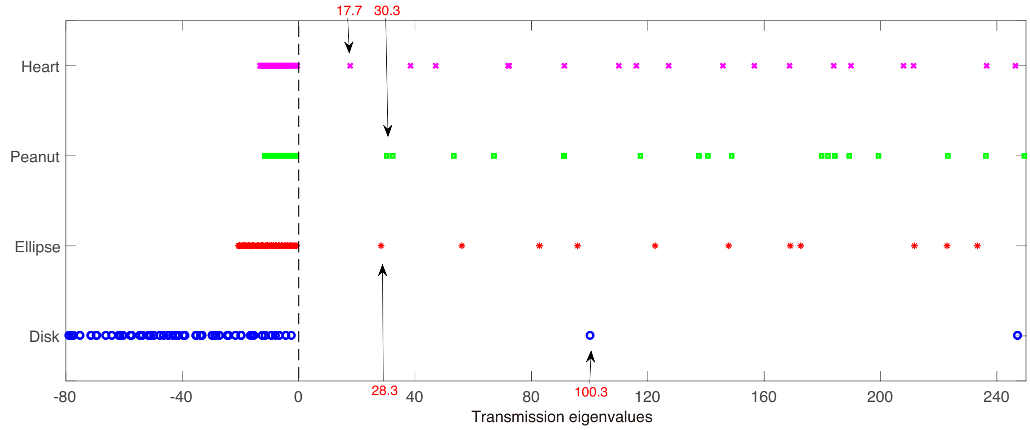

Figure 3. The eigenvalues λ of the QEP (18) in the intervel $[-80, 250]$ for the four domains in Figure 2 with $\varepsilon(\mathbf{x}) = -100$. The arrows point to the first positive eigenvalue of the QEP corresponding to each domain.

Davidson method in [23] to solve these QEPs. Of course, the partial locking and partial deflation schemes of Algorithm 2 and Algorithm 3 in [23] can be employed as well. The numerical results are shown in Figure 3.

Owing to the negative inhomogeneous medium $\varepsilon(\mathbf{x}) = \varepsilon_r - (\gamma_1^2 + \gamma_2^2)$ in TEP (1) derived from the pesudo-chiral model. From Figure 3, we immediately observe that there indeed exists an eigenvalue-free interval $(0, \beta^*) = (0, 100.3)$ (disk), $(0, 28.3)$ (ellipse), $(0, 30.3)$ (peanut) and $(0, 17.3)$ (heart), which verifies Theorem 3.5. Consequently, it is legitimate to say that k^2 is not a transmission eigenvalue if $k^2 \in (0, \beta^*)$. In comparison, we note that the TEP (1a) with the Tellegen model in [23] is reduced to

$$-\Delta E_3 = \omega^2(\varepsilon_r + (\gamma_1^2 + \gamma_2^2))E_3 \equiv \omega^2\varepsilon(\mathbf{x})E_3 \tag{43}$$

with a large positive inhomogeneous medium $\varepsilon(\mathbf{x})$, and its transmission eigenvalues are densely distributed on the interval $(0, O(1))$.

5.2. Reconstruction of the unknown domain from the near-field measurements

In this subsection, we apply Algorithm 1 to reconstruct the domain D from the near-field measurements for four distinct shapes as in Figure 2. As described above, our method is based on the LSM and the SVD technique.

For LSM, as shown in Figure 1, we make the following preparations for numerical experiments. Consider each domain in Figure 2 to be the target D, and let the circles with radii 3 and 6 be Γ and C, respectively. Choose the rectangle domain $[-1,1]\times[-1,1]$ to be the sampling domain T, which contains all possible targets D. From Figure 3, we choose a $k \in (0, \sqrt{\beta^*})$, in other words, k^2 is not a transmission eigenvalue. Different $k \in (0, \sqrt{\beta^*})$'s are chosen for testing in our numerical simulations.

Divid C and Γ into m and n segments uniformly, and denote the nodes as $\mathbf{x}_1, \cdots, \mathbf{x}_m$ and $\mathbf{y}_1, \cdots, \mathbf{y}_n$, respectively. Place a uniform grid on T by drawing vertical and horizontal lines through the points with coordinates (x_{1i}, x_{2j}), where $x_{1i} = -1 + ih_1$ for $i = 1, \cdots, p$ and $x_{2j} = -1 + jh_2$ for $j = 1, \cdots, q$, respectively. Let each mesh point (x_{1i}, x_{2j}) to be the sampling point $\mathbf{z}_{ij}$. In our experiment, for these parameters, we choose $m = 1269$, $n = 693$ and $p = q = 201$, respectively.

To construct the discretized near-field integral equation, we need to collect all the scattered fields u^s on the detection points $\mathbf{y}_1, \cdots, \mathbf{y}_n$ for each point source $\mathbf{x}_i$, $i = 1, \cdots, m$. For the purpose of numerical experiments, for a given point source $\mathbf{x}_i$, we can obtain the scattered fields in row $[u^s_{i1}, \cdots, u^s_{in}]$ by solving the direct scattering problem (2) using the FEM in Appendix A. Here, the FEM is applied to the domain enclosed by C, and the corresponding dimensions of E in Table 1 are $n = 143834$ and $m = 1269$, respectively. Adding 3% noise to the computed scattered fields u^s to produce the detected waves, with which, we discretize (32) into an ill-posed overdetermined linear system (33) with $A = [\delta_\Gamma u^s_{ij}(\mathbf{x}_i, \mathbf{y}_j)]_{m\times n} \in \mathbb{C}^{m\times n}$, where $\delta_\Gamma = 6\pi/n$ is the arc length of the uniform segment of Γ .

Applying Algorithm 1 to each sampling point $\mathbf{z}_{ij} \in T$ with all the above parameters to obtain the corresponding indicator $I_{\mathbf{z}_{ij}}$ for $i = 1, \cdots, p$ and $j = 1, \cdots, q$. From numerous numerical experiments by tuning $k \in (0, \sqrt{\beta^*})$, we find that the reconstruction results will be heavily affected by the wave number k. In Figure 4, we show the 3d surface figures and the corresponding 2d contour figures by plotting $I_{\mathbf{z}_{ij}}$ with respect to $(\mathbf{x}_i, \mathbf{y}_j) \in T$, and the actual targets in Figure 2 are plotted by red lines. In fact, Figure 4 shows the best results for reconstructing targets listed in Figure 2 by choosing appropriate wave numbers $k^* \in (0, \sqrt{\beta^*})$. In Figure 5, we show the 2d contour figures for other wave numbers $k \in (0, \sqrt{\beta^*})$. According to our experimental experience, the areas of the reconstructed domains are less than the areas of the actual domains by approximately $10\% - 20\%$. Our numerical experiments also suggest that the reconstructions of convex domains are more stable with respect to the choice of the wave number k and noise.

5.3. Tellegen model – positive index of refraction

In comparison, we demonstrate some numerical results of reconstructing the unknown target D for the inverse scattering problem with positive index of refraction. In [24], we considered the Maxwell's equations with the TM mode in Tellegen media and derived the acoustic equation (1a) with a positive $\varepsilon(\mathbf{x})$ increasing with respect to the Tellegen parameters. When $\varepsilon(\mathbf{x})$ is large enough, we have shown that the transmission eigenvalues are densely distributed near the origin. In this subsection, we show some numerical

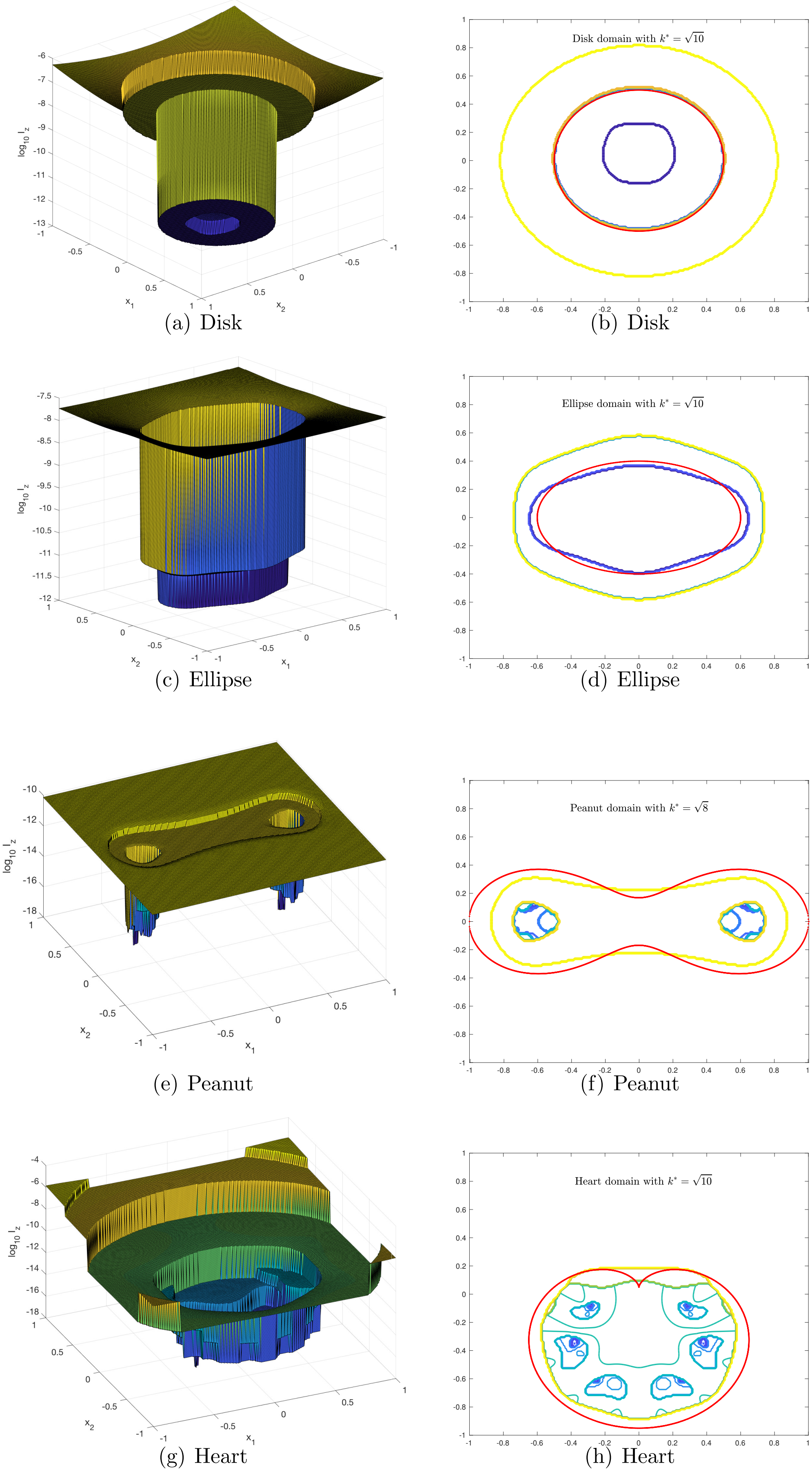

(a) Disk (b) Disk

(c) Ellipse (d) Ellipse

(e) Peanut (f) Peanut

(g) Heart (h) Heart

Figure 4. Reconstruction results of four targets in 3d surface figures and in 2d contour figures with $\varepsilon(\mathbf{x}) = -100$ and $k^* \in (0, \sqrt{\beta^*})$. The domains enclosed by red curves are the exact targets D. The scattered fields used have 3% noise.

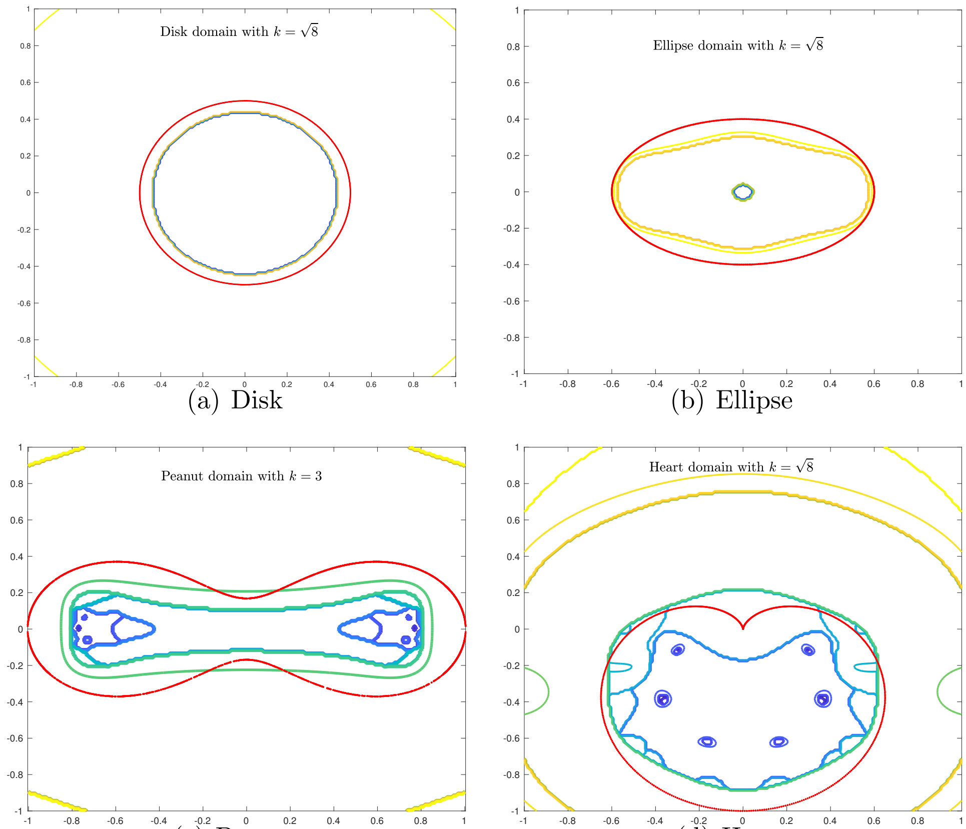

(a) Disk (b) Ellipse (c) Peanut (d) Heart

Figure 5. Reconstruction results of four targets in 2d contour figures with $\varepsilon(\mathbf{x}) = -100$ and the different $k \in (0, \sqrt{\beta^*})$. The domains enclosed by red curves are the exact targets D. The scattered fields have 3% noise.

reconstruction results based on our method when k^2 is an eigenvalue of the associated QEP (presumably a transmission eigenvalue). We test two different kinds of index of refraction on the disk domain, one is a normal index of refraction $\varepsilon(\mathbf{x}) = 16$ [24] and the other is $\varepsilon(\mathbf{x}) = 500$ (Tellegen model) [23]. As shown in [24], when $\varepsilon(\mathbf{x}) = 16$, the lowest transmission eigenvalue is approximately 1.988. In Figure 6(a), 6(b), we see that the reconstruction results are very sensitive to the choice of the wave number k. For the case of $\varepsilon(\mathbf{x}) = 500$, our numerical result in [23] indicates that the transmission eigenvalues are distribute densely in the interval $(0, 50)$. Figure 6(c) (choosing $k = 5$) shows that the disk is completely unrecognizable. The numerical results in this subsection verify the need of avoiding the transmission eigenvalues in the LSM.

6. Conclusion

In this paper, we propose a practical numerical method based on the LSM and the truncated SVD to reconstruct the support of the inhomogeneity in the acoustic equation with negative index of refraction, resulting from in pseudo-chiral media. It turns out

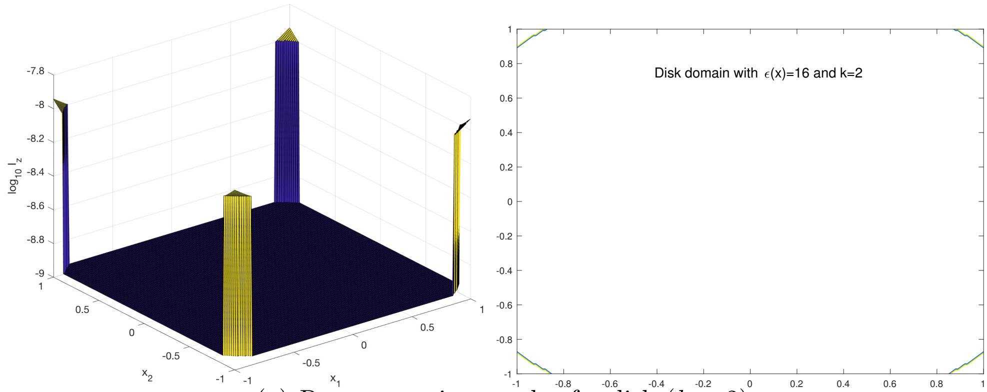

(a) Reconstruction result of a disk ($k = 2$)

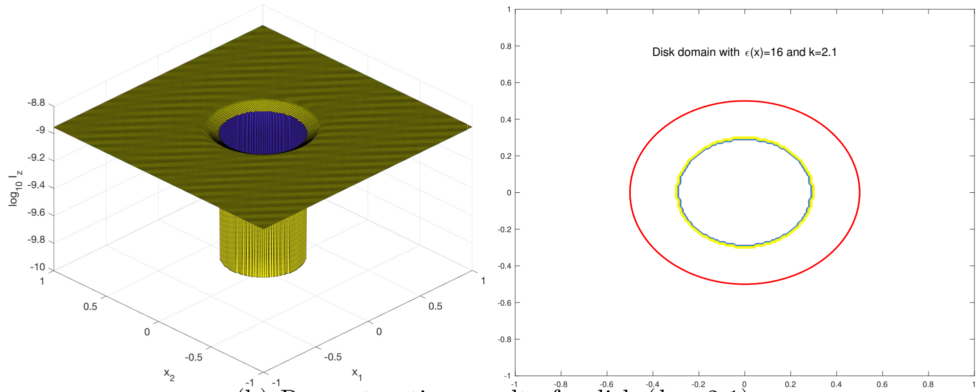

(b) Reconstruction result of a disk ($k = 2.1$)

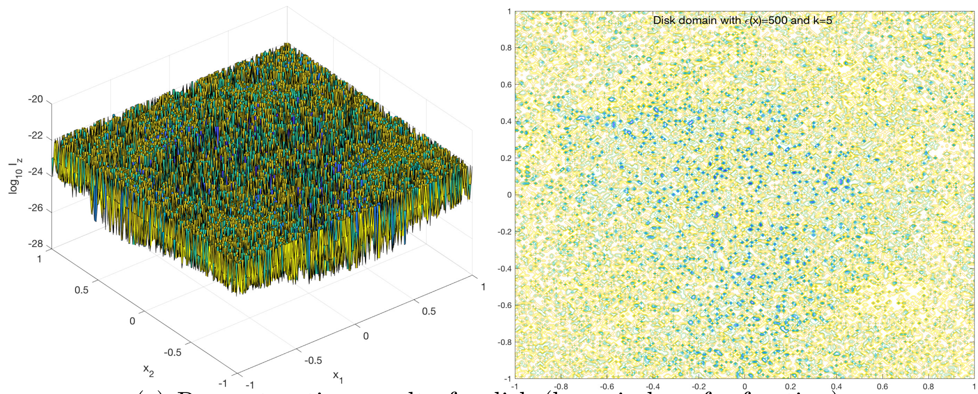

(c) Reconstruction result of a disk (large index of refraction)

Figure 6. Numerical reconstruction results of a disk when k^2 is a transmission eigenvalue. The scattered fields have 3% noise.

the index of refraction is in the form $\varepsilon(\mathbf{x}) = \varepsilon_r - (\gamma_1^2 + \gamma_2^2)$. We are also interested in the distribution of transmission eigenvalues for the corresponding TEP. The associated discretized TEP can be reduced into a QEP with symmetric coefficient matrices whose all the nonphysical zero eigenvalues are deflated. We prove that the corresponding QEP has half of negative eigenvalues and half of positive eigenvalues in $(-\beta_*, 0)$ and (β^*, ∞), respectively, and there exists an eigenvalue-free interval $(0, \beta^*)$. We then apply the LSM using the near-field data to reconstruct the domain D with $\varepsilon(\mathbf{x}) \neq 1$ and propose an easily implemented truncated SVD technique to determine whether a sampling point is inside or outside of D according to the size of the indicator function. Numerical results show that the effectiveness of our method depends on the wave numbers of incident fields and the convexity of the target.

7. Acknowledgments

Li is supported in parts by the NSFC 11471074. Huang was partially supported by the Ministry of Science and Technology (MOST) 105-2115-M-003-009-MY3, National Center of Theoretical Sciences (NCTS) in Taiwan. Lin was partially supported by MOST, NCTS and ST Yau Center in Taiwan. Wang was partially supported by MOST 105-2115-M-002-014-MY3.

Appendix A. An FEM framework for the direct scattering problem

In this appendix, we will present a numerical framework of solving the direct scattering problem (2) by the FEM given in Section 3. As described in Figure 1, let $u^i = \Phi(\mathbf{x}, \mathbf{x}_0)$ be an incident field with $\mathbf{x}_0 \in C$. Suppose C is far from the origin, since $\Delta u^i + k^2 u^i = 0$, we have

$$\begin{aligned} &\Delta(u^i + u^s) + k^2\varepsilon(\mathbf{x})(u^i + u^s) \\ =&\Delta u^s + k^2\varepsilon(\mathbf{x})u^s + \Delta u^i + k^2 u^i + k^2(\varepsilon(\mathbf{x}) - 1)u^i \\ =&(\Delta + k^2\varepsilon(\mathbf{x}))u^s + k^2(\varepsilon(\mathbf{x}) - 1)u^i = 0, \quad \mathbf{x} \in \mathbb{R}^2 \setminus \{\mathbf{x}_0\}, \quad \mathbf{x}_0 \in C, \end{aligned} \tag{44a}$$

and

$$\frac{\partial u^s}{\partial r} = \mathrm{i}ku^s|_C. \tag{44b}$$

Denote $\bar{C}$ the closed domain enclosed by C. Applying the standard FEM framework in Section 3 on $\bar{C}$, we define in addition the stiffness matrix for boundary meshes as

$$S = [(\nabla\psi_i, \nabla\psi_j)] \succ 0 \in \mathbb{R}^{m\times m}, \tag{45}$$

and the mass matrices for boundary condition as

$$R = [\int_C \psi_i\psi_j ds] = [\frac{1}{6}(1 + \delta_{ij})|e_{ij}|] \succ 0 \in \mathbb{R}^{m\times m}, \tag{46}$$

where $|e_{ij}|$ is the length of boundary edge e_{ij} and δ_{ij} being the Kronecker delta function. Let

$$u^s = \sum_{i=1}^{n} w_i\phi_i + \sum_{i=1}^{m} v_i\psi_i,$$

and

$$u^i = \Phi(\mathbf{x}, \mathbf{x}_0) = \sum_{i=1}^{n} f_i\phi_i + \sum_{i=1}^{m} g_i\psi_i,$$

it follows from (44a) that

$$
\begin{aligned}
0 =&((\Delta + k^2\varepsilon(\mathbf{x}))u^s, \phi_j) + (k^2(\varepsilon(\mathbf{x}) - 1)u^i, \phi_j) \\
=&(\Delta u^s, \phi_j) + k^2(\varepsilon(\mathbf{x})u^s, \phi_j) + k^2(\varepsilon(\mathbf{x})\Phi(x, x_0), \phi_j) - k^2(\Phi(\mathbf{x}, \mathbf{x}_0), \phi_j).
\end{aligned} \tag{47}
$$

Utilizing the integration by parts and setting $\mathbf{w} = [w_1, \cdots, w_n]^\top$, $\mathbf{v} = [v_1, \cdots, v_m]^\top$, $\mathbf{f} = [f_1, \cdots, f_n]^\top$ and $\mathbf{g} = [g_1, \cdots, g_m]^\top$, (47) can be written as

$$
\begin{aligned}
&(\Delta u^s, \phi_j) + k^2(\varepsilon(\mathbf{x})u^s, \phi_j) \\
=& - (\nabla u^s, \nabla\phi_j) + k^2(\varepsilon(\mathbf{x})u^s, \phi_j) \\
=& - \left(\sum_{i=1}^{n} w_i(\nabla\phi_i, \nabla\phi_j) + \sum_{i=1}^{m} v_i(\nabla\psi_i, \nabla\phi_j)\right) + k^2\left(\sum_{i=1}^{n} w_i(\varepsilon\phi_i, \phi_j) + \sum_{i=1}^{m} v_i(\varepsilon\psi_i, \phi_j)\right) \\
=& - \left(\sum_{i=1}^{n} w_i K_{ij} + \sum_{i=1}^{m} v_i E_{ji}\right) - k^2\left(\sum_{i=1}^{n} w_i M_{\varepsilon ij} + \sum_{i=1}^{m} v_i F_{\varepsilon ji}\right) \\
=& - K\mathbf{w} - E\mathbf{v} - k^2 M_\varepsilon \mathbf{w} - k^2 F_\varepsilon \mathbf{v},
\end{aligned} \tag{48}
$$

and

$$
\begin{aligned}
&k^2(\varepsilon(\mathbf{x})\Phi(\mathbf{x}, \mathbf{x}_0), \phi_j) - k^2(\Phi(\mathbf{x}, \mathbf{x}_0), \phi_j) \\
=&k^2\left(\sum_{i=1}^{n} f_i(\varepsilon\phi_i, \phi_j) + \sum_{i=1}^{m} g_i(\varepsilon\psi_i, \phi_j)\right) - k^2\left(\sum_{i=1}^{n} f_i(\phi_i, \phi_j) + \sum_{i=1}^{m} g_i(\psi_i, \phi_j)\right) \\
=& - k^2\sum_{i=1}^{n} f_i M_{\varepsilon ij} - k^2\sum_{i=1}^{m} g_i F_{\varepsilon ji} - k^2\sum_{i=1}^{n} f_i M_{1ij} - k^2\sum_{i=1}^{m} g_i F_{1ji} \\
=& - k^2(M_\varepsilon + M_1)\mathbf{f} - k^2(F_\varepsilon + F_1)\mathbf{g},
\end{aligned} \tag{49}
$$

where the stiffness matrices K, E and mass matrices M_1, M_ε, F_1, F_ε are defined as in Table 1 with domain D being replaced by $\bar{C}$.

Continuing to apply the FEM and integration by parts to (44a), combining with

(44b), we obtain that

$$\begin{aligned}
&(\Delta u^s,\psi_j)+k^2(\varepsilon(\mathbf{x})u^s,\psi_j)\\
=&-(\nabla u^s,\nabla\psi_j)+\int_C \nabla_{\mathbf{n}}u^s\psi_j ds+k^2(\varepsilon(\mathbf{x})u^s,\psi_j)\\
=&-\left(\sum_{i=1}^n w_i(\nabla\phi_i,\nabla\psi_j)+\sum_{i=1}^m v_i(\nabla\psi_i,\nabla\psi_j)\right)+\int_C \mathrm{i}ku^s\psi_j ds\\
&+k^2\left(\sum_{i=1}^n w_i(\varepsilon\phi_i,\psi_j)+\sum_{i=1}^m v_i(\varepsilon\psi_i,\psi_j)\right)\\
=&-\sum_{i=1}^n w_iE_{ij}-\sum_{i=1}^m v_iS_{ij}+\mathrm{i}k\left(\sum_{i=1}^n w_i\int_C\phi_i\psi_j ds+\sum_{i=1}^m v_i\int_C\psi_i\psi_j ds\right)\\
&-k^2\left(\sum_{i=1}^n w_iF_{\varepsilon ij}+\sum_{i=1}^m v_iG_{\varepsilon ij}\right)\\
=&-(E^T+k^2F_\varepsilon^T)\mathbf{w}-(S+k^2G_\varepsilon)\mathbf{v}+\mathrm{i}kR\mathbf{v}
\end{aligned}\tag{50}$$

and

$$\begin{aligned}
&k^2(\varepsilon(\mathbf{x})\Phi(\mathbf{x},\mathbf{x}_0),\psi_j)-k^2(\Phi(\mathbf{x},\mathbf{x}_0),\psi_j)\\
=&k^2\left(\sum_{i=1}^n f_i(\varepsilon\phi_i,\psi_j)+\sum_{i=1}^m g_i(\varepsilon\psi_i,\psi_j)\right)-k^2\left(\sum_{i=1}^n f_i(\phi_i,\psi_j)+\sum_{i=1}^m g_i(\psi_i,\psi_j)\right)\\
=&-k^2\sum_{i=1}^n f_iF_{\varepsilon ij}-k^2\sum_{i=1}^m g_iG_{\varepsilon ij}-k^2\sum_{i=1}^n f_iF_{1ij}-k^2\sum_{i=1}^m g_iG_{1ij}\\
=&-k^2(F_1^T+F_\varepsilon^T)\mathbf{f}-k^2(G_1+G_\varepsilon)\mathbf{g},
\end{aligned}\tag{51}$$

where S and R are given in (45) and (46), and similarly, the mass matrices G_1 and G_ε are defined as in Table 1 on domain $\bar{C}$. Finally, we can arrange (48), (49), (50) and (51) into a linear system

$$\begin{bmatrix} K+k^2M_\varepsilon & E+k^2F_\varepsilon \\ E^T+k^2F_\varepsilon^T & S+k^2G_\varepsilon-\mathrm{i}kR\end{bmatrix}\begin{bmatrix}\mathbf{w}\\ \mathbf{v}\end{bmatrix}=-k^2\begin{bmatrix} M_\varepsilon+M_1 & F_1+F_\varepsilon \\ F_1^T+F_\varepsilon^T & G_1+G_\varepsilon\end{bmatrix}\begin{bmatrix}\mathbf{f}\\ \mathbf{g}\end{bmatrix}. \tag{52}$$

The approximate scattered field u^s is then obtained by solving (52).

References

[1] F. Cakoni and D. Colton. *Qualitative methods in inverse scattering theory: An introduction.* Springer Science & Business Media, 2005.

[2] F. Cakoni, D. Colton, and H. Haddar. On the determination of Dirichlet or transmission eigenvalues from far field data. *C. R. Math. Acad. Sci. Pairs*, 348(7-8):379–383, 2010.

[3] F. Cakoni, D. Colton, P. Monk, and J. Sun. The inverse electromagnetic scattering problem for anisotropic media. *Inv. Prob.*, 26(7):074004, 2010.

[4] F. Cakoni, D. Gintides, and H. Haddar. The existence of an infinite discrete set of transmission eigenvalues. *SIAM J. Math. Anal.*, 42(1):237–255, 2010.

[5] F. Cakoni and H. Haddar. On the existence of transmission eigenvalues in an inhomogeneous medium. *Appl. Anal.*, 88(4):475–493, 2009.

[6] F. Cakoni and H. Haddar. Transmission eigenvalues in inverse scattering theory. In G. Uhlmann, editor, *Inverse Problems and Applications: Inside Out II*, volume 60 of *Math. Sci. Res. Inst. Publ.*, pages 527–578. Cambridge University Press, Cambridge, 2012.

[7] D. Colton and H. Haddar. An application of the reciprocity gap functional to inverse scattering theory. *Inv. Prob.*, 21:383–98, 2005.

[8] D. Colton and A. Kirsch. A simple method for solving inverse scattering problems in the resonance region. *Inv. Prob.*, 12(4):383, 1996.

[9] D. Colton and R. Kress. *Inverse Acoustic and Electromagnetic Scattering Theory*, volume 93 of *Applied Mathematical Sciences*. Springer, New York, 3rd edition, 2013.

[10] D. Colton and P. Monk. A novel method for solving the inverse scattering problem for time-harmonic acoustic waves in the resonance region. *SIAM J. Appl. Math.*, 45:1039–53, 1985.

[11] D. Colton, P. Monk, and J. Sun. Analytical and computational methods for transmission eigenvalues. *Inv. Prob.*, 26:045011, 2010.

[12] D. Colton, L. Päivärinta, and J. Sylvester. The interior transmission problem. *Inv. Prob. Imaging*, 1(1):13–28, 2007.

[13] P.C. Hansen. *Discrete Inverse Problems: Insight and Algorithms.* SIAM, Philadelphia, PA, 2010.

[14] G. C. Hsiao, F. Liu, J. Sun, and L. Xu. A coupled BEM and FEM for the interior transmission problem in acoustics. *J. Comput. Appl. Math.*, 235:5213–5221, 2011.

[15] T.-M. Huang, W.-Q. Huang, and W.-W. Lin. A robust numerical algorithm for computing Maxwell's transmission eigenvalue problems. *SIAM J. Sci. Comput.*, 37:A2403–A2423, 2015.

[16] T.-M. Hwang, W.-W. Lin, W.-C. Wang, and W. Wang. Numerical simulation of three dimensional pyramid quantum dot. *J. Comput. Phys.*, 196:208–232, 2004.

[17] X. Ji, J. Sun, and T. Turner. Algorithm 922: A mixed finite element method for Helmholtz transmission eigenvalues. *ACM Trans. Math. Software*, 38:29, 2012.

[18] X. Ji, J. Sun, and H. Xie. A multigrid method for Helmholtz transmission eigenvalue problems. *J. Sci. Comput.*, 60(2):276–294, 2014.

[19] M.E. Kilmer and D.P. O'leary. Choosing regularization parameters in iterative methods for ill-posed problems. *SIAM J. Matrix Anal. Appl.*, 22(4):1204–1221, 2001.

[20] A. Kirsch. On the existence of transmission eigenvalues. *Inv. Prob. Imaging*, 3(2):155–172, 2009.

[21] A. Kirsch and N. Grinberg. *The factorization method for inverse problems.* Number 36. Oxford University Press, 2008.

[22] A. Kleefeld. *Numerical methods for acoustic and electromagnetic scattering: Transmission boundary-value problems, interior transmission eigenvalues, and the factorization method.* Habilitation Thesis, May 2015.

[23] T. Li, T. M. Huang, W. W. Lin, and J. N. Wang. An efficient numerical algorithm for computing densely distributed positive interior transmission eigenvalues. *Inv. Prob.*, 33:035009, 2017.

[24] T. Li, W.-Q. Huang, W.-W. Lin, and J. Liu. On spectral analysis and a novel algorithm for transmission eigenvalue problems. *J. Sci. Comput.*, 64(1):83–108, 2015.

[25] L. Päivärinta and J. Sylvester. Transmission eigenvalues. *SIAM J. Math. Anal.*, 40(2):738–753, 2008.

[26] A. Serdyukov, I. Semchenko, S. Tretyakov, and A. Sihvola. *Electromagnetics of Bi-anisotropic Materials: Theory and Applications.* Gordon and Breach Science, 2001.

[27] J. Sun. Estimation of transmission eigenvalues and the index of refraction from cauchy data. *Inv. Prob.*, 27(1):015009, 2010.

[28] J. Sun. Iterative methods for transmission eigenvalues. *SIAM J. Numer. Anal.*, 49(5):1860–1874, 2011.

[29] J. Sun. An eigenvalue method using multiple frequency data for inverse scattering problems. *Inv.*

Prob., 28(2):025012, 2012.

[30] J. Sun and A. Zhou. *Finite Element Methods for Eigenvalue Problems.* Boca Raton: CRC Press, 2017.

[31] A.N. Tikhonov and V.Y. Arsenin. *Solutions of Ill-Posed Problems.* Winston Sons, Washington, D.C., 1977.